



Contents lists available at ScienceDirect

Chemical Engineering Science

journal homepage: <http://ees.elsevier.com>



Sustainable preparation of graphene-like hybrid nanomaterials and their application for organic dyes removal

Samia Mahouche-Chergui^{a,*}, Zakariae Boussaboun^b, Abdallah Oun^a, Maryam Kazembeyki^c, Christian G. Hoover^c, Benjamin Carbonnier^a, Claudiane M. Ouellet-Plamondon^{b,*}

^a Univ Paris Est Creteil, CNRS, ICMPE, UMR 7182, 2 rue Henri Dunant, 94320 Thiais, France

^b École de Technologie Supérieure, University of Québec, Montréal, QC, Canada

^c School of Sustainable Engineering and the Built Environment, Arizona State University, Tempe, AZ 85287, USA

ARTICLE INFO

Article history:

Received 14 May 2020

Received in revised form 6 January 2021

Accepted 20 January 2021

Available online xxx

Keywords

Graphene

Renewable precursors

Graphene-bentonite hybrid nanomaterial

Nanoindentation

Pollutants removal

ABSTRACT

Graphene-like hybrid nanomaterials (GHNs) were successfully synthesized through a sustainable and solvent-free method. Sucrose and bentonite renewable precursors were used as a carbon source and a template, respectively. The characterization of GHN by Raman nanoscale spectroscopy and X-ray photoelectron spectroscopy (XPS) confirmed the successful transformation of sucrose to sp²-hybridized carbon as in graphene. The high-resolution transmission electron microscopy (HR-TEM) analysis evidenced the formation of a hybrid nanomaterial in a well-defined layered structure. The nanoindentation studies show that the modulus of the pyrolyzed sugar was 4 GPa, while it was 28 GPa for the graphene layer synthesized with this procedure. These hybrid nanomaterials were evaluated as an adsorbent for the removal of both cationic (rhodamine B and methylene blue dyes) and anionic (methyl orange) organic water pollutants at 9.5–10 mg/g. These stiffer GHN increase the resilience, durability, and sustainability of the clay particles for treatment processes.

© 2021

1. Introduction

During the past two decades, research on graphene has progressed rapidly. Specific attention has been given to advancing the processes that transform graphite into monolayer carbon, including spray methods (Bi et al., 2019) and sol gel-based processes (Chen et al., 2019; Wang et al., 2019). Layered double oxides (Shahzad et al., 2019) have also been used, but these processes are still dependent on chemical treatments similar to conventional technology at the laboratory scale. The intercalation of graphene oxide within inorganic substrates have shown superior adsorption capacities using anchored, or intercalated, graphene particles within inorganic substrates (Shahzad et al., 2019). Clay-supported graphene materials have been identified as promising adsorbents for hydrogen storage applications (Ruiz-Garcia et al., 2013) and for sustainable dielectric composites (Azizi, 2017) (Azizi, 2019). Clays are abundant, inexpensive, eco-friendly and active surface materials (Unuabonah et al., 2013). Their layered structure leads to porous hybrid nanomaterials with favorable properties for graphene formation (Ruiz-Hitzky et al., 2016) within the clay layers.

Facile and cost-efficient processes are still needed in order to bring these advances to industrial applications. Another point of inquiry is what readily available functional materials are available and able to support the formation of graphene layers from renewable carbon source precursors (Ruiz-Garcia et al., 2013; Chyan et al., 2018; Ruan et al., 2011; Ruiz-Garcia et al., 2014). Pulse lasers can transform many renewable organic substrates into laser-induced graphene (Chyan et al., 2018). While this method is sound, the ability for it to be upscaled to large volumes is very expensive and time consuming. Pyrolysis remains a scalable approach to produce carbonaceous materials from renewable precursors (Wang et al., 2019).

In water treatment, the presence of recalcitrant compounds, such as organic dyes, are of particular concern because of their toxicity that causes health risks to humans. Adsorption on natural minerals is well-known (Krstić et al., 2018). Graphene based nanomaterials have been reported to improve the decontamination of heavy metals (Krstić et al., 2018; Perreault et al., 2015), anionic and cationic dyes (Xiao et al., 2016), pharmaceuticals (Wang et al., 2019; Al-Hamadani et al., 2017), and other organic compounds (Chen et al., 2019; Perreault et al., 2015). The implementation of these technologies has been limited by the expensive and complicated synthesis procedures (Bi et al., 2019; Chen et al., 2019; Shahzad et al., 2019; Perreault et al., 2015). To overcome these issues, graphene-clay-based nanomaterials prepared by inert pyrolysis of renewable low cost and natural products can be employed. Bentonite clay is often used in large-

Abbreviations: GHN, graphene hybrid nanomaterial.

* Corresponding authors.

E-mail addresses: mahouche-chergui@icmpe.cnrs.fr (S. Mahouche-Chergui); claudiane.ouellet-plamondon@etsmtl.ca (C.M. Ouellet-Plamondon)

scale engineering applications. The graphene can provide additional mechanical stiffness to the clay particles, which increases the resilience, durability and sustainability of the particles themselves.

In this article, a multilayered graphene intercalated into a natural porous bentonite is made using a cost-effective, facile and scalable method. Here in, we use sucrose, which is a disaccharide consisting of a molecule of glucose united with a molecule of fructose (Zhu et al., 2010). In this study, bentonite is used as an inorganic porous substrate because it is commonly used in civil engineering for large-scale projects and it is widely available. The bentonite contains montmorillonite clay, which consists of octahedral layers sandwiched between two tetrahedral sheets, and is the template material in the production of these graphene-like clay nanocomposite (Ruiz-Hitzky et al., 2016; Ruiz-Garcia et al., 2014; Rahmani and Nouranian, 2018; Li et al., 2016; Cheng et al., 2017). The silicate layers of montmorillonite contain negative charges that must be stabilized by inorganic cations or contact with water (Segad et al., 2010). Graphene-like hybrid clay nanomaterials have a synergic effect and they can be used for many polymer applications (Bouakaz et al., 2017, 2015). The advantage of this materials is that it can be produced with readily available materials, clays and sugar. Nanostructured materials tend to have a better affinity to adsorb pollutants. However, the mechanism of the transformation from sugar to graphitized carbon still has open questions.

The biggest challenge of the large-scale production of hybrid graphene materials from natural resources is controlling the transformation reaction of precursors to graphene-like materials on porous solids while maintaining cost effectiveness and scalability. Raman spectroscopy, X-ray photoelectron spectrometry (XPS), and high-resolution transmission electron microscopy (HR-TEM) and were used to confirm that this method promoted the graphitization of sucrose in the bentonite network. The influence of these graphene-like layers on the development of mechanical properties of the bentonite composites, namely elasticity and strength, have not – to the best of our knowledge – been addressed in the open literature. Herein, the local mechanical properties of the synthesized materials (pure and composites) were investigated using an indentation technique to determine their indentation modulus (M) and hardness (H) at the submicrometer scale. The nanoindentation measurements allowed to better understand the phases in the composite graphene-like clay, to quantify the improved mechanical properties due to the presence of the graphene and to provide recommendations for process improvements. In order to evaluate the adsorption performances of the designed bentonite-graphene hybrid

nanomaterials (GHN), the removal of three organic dyes, rhodamine B (RhB), methylene blue (MB) and methyl orange (MO) was studied. Efforts were devoted to study the adsorption kinetics and recyclability of adsorbent through chemical regeneration.

2. Experimental section

2.1. Materials

The sodium bentonite (BT) was obtained from Canadian Clay Products, Inc (65–85 meq/100 g ion-exchange capacity, 75.88 m²/g surface area, 2.6 g/cm³ density) and used without further treatment. The chemical composition was SiO₂ 67.1%, Al₂O₃ 16.43%, MgO 2.09%, Fe₂O₃ 7.76%, CaO 1.30%, K₂O 1.55%, Na₂O 2.32%, TiO₂ 0.43%. All chemicals, including saccharose (C₁₂H₂₂O₁₁, 99.5%), methylene blue (MB, >97%), rhodamine B (RhB, >95%), and the methyl orange (MO, >97%) were purchased from Sigma-Aldrich and used as received. The 0.1 N sodium hydroxide (NaOH) and 0.1 N hydrochloric acid (HCl) were purchased from VWR Chemicals BDH Prolabo. The aqueous solutions used in this work were prepared with Millipore water (DI water).

2.2. Preparation of graphene-like hybrid nanomaterial (GHN)

Graphene-like hybrid nanomaterial was prepared according to our previously described eco-friendly method where natural clay and saccharose were used as precursor materials (Fig. 1) (Boussaboun et al., 2017). Firstly, homogenized BT particles (less than 2 μm) were vigorously dispersed in DI water at 83.3% by weight. After 24 h of swelling at room temperature, the resulting suspension was mixed for 20 min with an aqueous solution of saccharose (2 g/mL by weight) in 1:5 wt ratio (BT: saccharose) using a mixer with a stirring speed of 400 rpm. Subsequently, the mixture was dried in an oven for 48 h at 50 °C, followed by an activation in a furnace at 800 °C for 1 h at a heating rate of 5 °C/min under nitrogen flow. Finally, the obtained dark monolith was ground using a mortar and pestle, then with a high-performance planetary ball mill (Pulverisette 6, Laval Lab Inc.) until the particle size is less than 20 μm.

2.3. Physicochemical characterizations

The graphitic structure of GHN was evaluated by Raman spectroscopy using alpha 300R confocal Raman microscope with a wavelength of 532 nm. The elemental composition of GHN was investigated

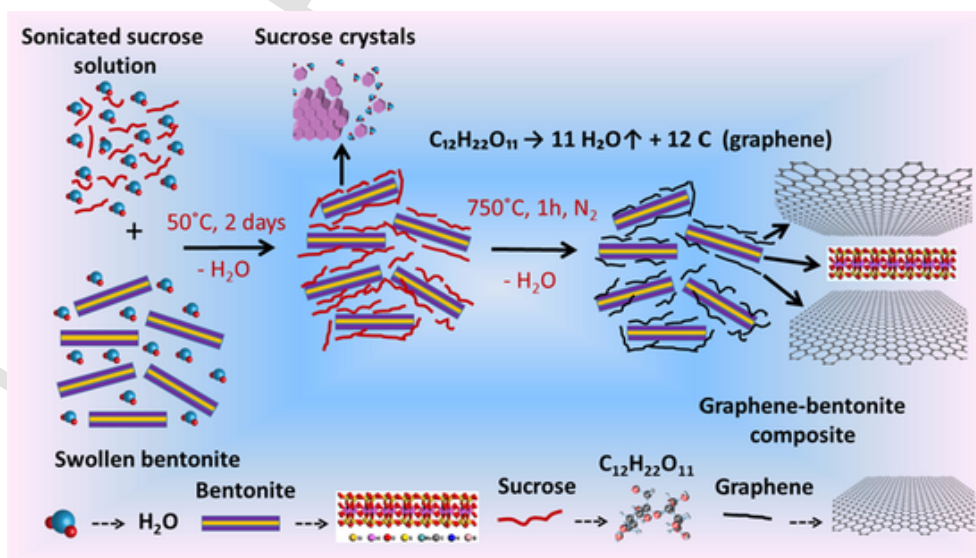


Fig. 1. Schematic illustration of the synthesis of the graphene-like hybrid nanomaterials from sucrose and natural bentonite.

by X-ray photoelectron spectroscopy (XPS) recorded on a Thermo Scientific K-Alpha spectrometer equipped with a monochromatic Al-K α X-ray source ($h\nu = 1486$ eV). The operation pressure was around 2×10^{-9} Torr and the spot size of the X-ray was 400 μm . The electron kinetic energy was determined using a hemispherical analyzer with a pass energy of 200 and 50 eV for survey and high-energy resolution scans, respectively. The morphology and microstructure of GHN were examined using transmission electron microscopy (TEM). HRTEM micrograph acquisitions were recorded using a JEOL 2170F at an accelerating voltage of 200 kV. Zeta potential measurements were performed using a Malvern Nano-ZS Zetasizer equipped with a He-Ne laser ($\lambda = 633$ nm). For each pH, the zeta potential was calculated as the average of three measurements of three subsequent runs. The concentrations of MB, RhB, and MO dyes in water were measured in 1 cm glass cuvettes using UV-Vis spectroscopy on an Agilent Cary 60 UV-Vis spectrophotometer.

Nanoindentation experiments were conducted to better understand the nanoscale mechanical properties of the GHN at submicrometer lengths. The particle-like sizes of the bentonite and graphene-like sheets had diameters that were no larger than 60 μm and required stabilization to ensure they remained stationary during the test. The particles were first dispersed and embedded in low-density polyethylene (LDPE) to provide the needed stabilization. The accuracy of the measurements requires a very smooth surface and isolation of the phase of interest (Miller et al., 2008; Oliver and Pharr, 2011a, 2011b). To ensure this, a polishing protocol was adopted that consisted of manual polishing using alumina pads with particle sizes of 9, 3 and 1 μm (Buehler, USA). The 9- μm particle size was used to remove the outer protective pure LDPE layer ($\sim 1\text{--}3$ μm thick) to expose the embedded bentonite and graphene-like sheets. The 3- and 1- μm alumina pads were then used to make the surface of the composite smooth and flat.

Before testing, the particle + LDPE composite samples were glued to a steel substrate to hold them in place for testing. Three samples were tested: Pure LDPE, LDPE + 10% bentonite, and LDPE + GHN. Only indents that were contained completely in one phase were considered for further analysis, curves landing on interfaces were excluded. Each indent was loaded in force control up to the limiting maximum load at a constant loading/unloading rate. At the peak load, the force was held constantly before the load was removed. In each phase, the loading parameters were optimized to ensure only the elastic response was dominating.

2.4. Adsorption of organic cationic and anionic dyes on GHN

In order to evaluate the adsorption characteristics of organic pollutants on the as-designed GHN, batch adsorption experiments were performed. For this, adsorption of three dyes was tested, methylene blue (MB), rhodamine B (RhB), and methyl orange (MO), where stock solutions of 1000 mg L $^{-1}$ were prepared from solid materials in deionized water. Twenty-five milligrams of GHN adsorbent were added to 10 mL of 25 mg L $^{-1}$ MB, RhB, or MO dye at pH 5 in 20 mL glass vial and the mixture was stirred for 60 min at 25 $^{\circ}\text{C}$ and then the supernatant was collected by centrifugation and analyzed with UV-Vis spectrophotometer. The initial pH of solutions was adjusted with 0.1 N HCl or 0.1 N NaOH. The effect of pH (2–10), temperature (25, 30, 40, and 50 $^{\circ}\text{C}$), and contact time (1–180 min) on the adsorption capacity of GHN was studied. All experiments were repeated three times with similar results. Adsorption capacity was calculated according to Eq. (1).

$$\text{Removal (\%)} = \frac{C_0 - C_e}{C_0} \times 100 \quad (1)$$

Here, C_0 and C_e are the initial and equilibrium concentrations of pollutants, respectively.

3. Results and discussion

3.1. Microstructure characterization

The conversion of sucrose-coated bentonite to graphene-like nanomaterial was demonstrated with Raman spectroscopy, a convenient tool for characterizing graphitic materials. As it can be observed from Fig. 2, the Raman spectrum of pure bentonite did not reveal any band in the wavenumber range of 1000–2000 cm^{-1} . The Raman spectra of pyrolyzed sugar exhibited a broad D-band (1372 cm^{-1}) and G-band (1585 cm^{-1}) while the 2D band was almost absent due to the low number of layers in the graphene structure (Oliveira et al., 2018). By adding bentonite, the D and G-band shifted to 1351 cm^{-1} and 1603 cm^{-1} , respectively. The Raman signal of pyrolyzed sugar was enhanced by ~ 8 fold by the presence of bentonite sheets due to the chemical modification of the carbon structure (Jasuja et al., 2010). The I_D/I_G ratio value decreased from 0.80 for pyrolyzed sugar to 0.67 for the GHM indicating a more ordered structure and a chemical binding between pyrolyzed sugar and bentonite in the GHM composite. Thus, the as-prepared GHM presents low defects compared to that found in literature (An et al., 2018; Eckmann et al., 2012).

The elemental composition of the GHN surface was investigated by XPS analysis. As expected, the XPS survey spectrum (Fig. 3a) of GHN contains the main peaks of Al 2p, Si 2p, C1s, and O1s, centered at 74, 102, 284, and 533 eV, respectively. The high-resolution spectrum of the C1s region (Fig. 3b) gives an asymmetric and complex peak, which is fitted with five components centered at 284.2, 285.6, 286.7, 288.5, and 290.5 eV, corresponding to sp^2 carbon (C = C), sp^3 carbon (C-C/C-H), C-O, C = O, and $\pi\text{-}\pi^*$ shake-up satellites, respectively. The high relative area of the sp^2 carbon peak (compared to that of sp^3) and the presence of the shake-up, which is characteristic of the aromatic compounds, clearly indicate the formation of graphene sheets from a renewable precursor using natural clay as a template. However, the presence of epoxy or alcohol groups (C-O-C, C-OH), carboxylic acid functions (HO-C = O), and sp^3 hybridized carbon (C-C, C-H) suggests the surface oxidation of a fraction of the graphene, which is in line with the high I_D/I_G ratio, as determined by Raman results (Boussaboun et al., 2017).

The microstructure of GHN was analyzed by high-resolution transmission electron microscopy (HRTEM). Fig. 4 reveals that GHN is organized in a sheet-like structure confirming the presence of graphene on the surface of bentonite layers, with a well combination between bentonite and graphene nanosheets. The 2D layered organization of

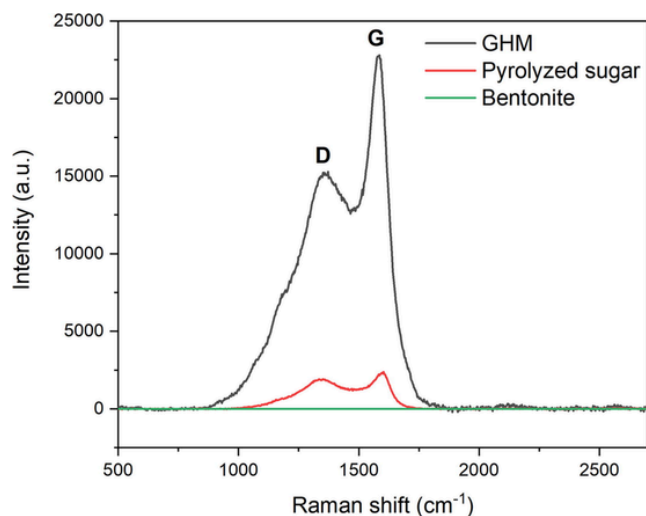


Fig. 2. Raman spectroscopy analysis of the bentonite compared to the GHN.

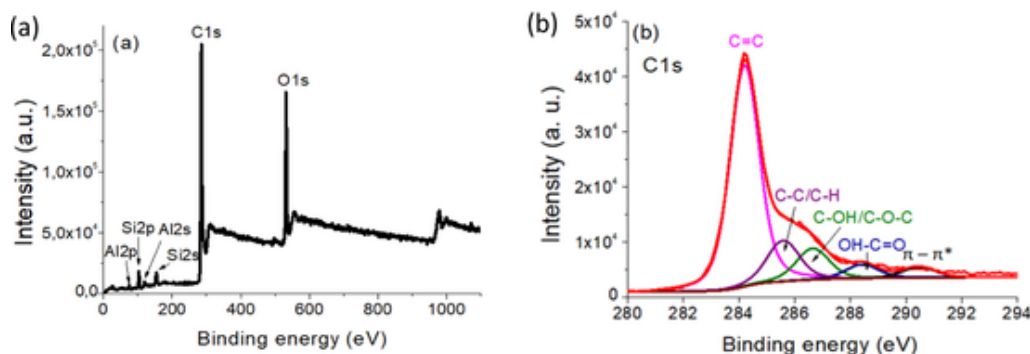


Fig. 3. Electron photo spectroscopy (a) survey scan and (b) deconvolution of C1s spectral peak of GHN.

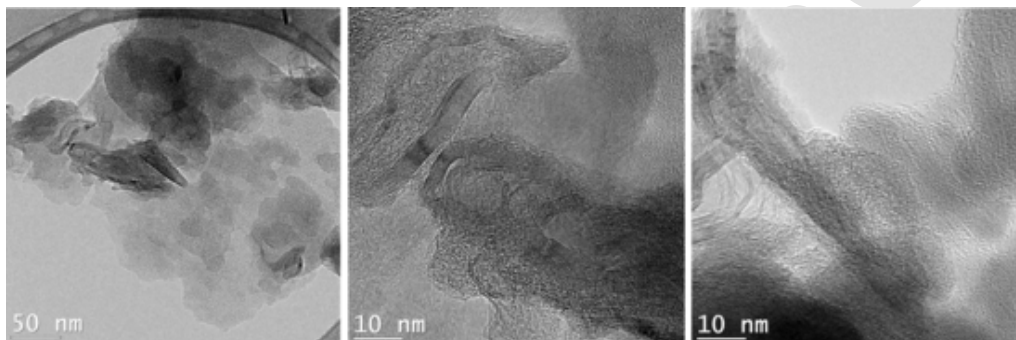


Fig. 4. HR-TEM at two magnifications of GHN.

GHN is induced by that of bentonite, the templating structure used during its synthesis. The GHN is composed from a mixture of multilayered and single-layer structure. The wavy graphene/bentonite sheets with has regions of individualized layers randomly dispersed when agglomerated multilayers are also observed.

3.2. Nanoscale mechanical properties

Nanoscale indentation tests were conducted to better understand the mechanical behavior of GHN. The tests were run using a loading and unloading rate of 0.3 mN/min with a hold time of 20 s after a max depth of 100 nm was reached. A minimum of 25 indents was performed. The output of the test is a force displacement (P-h) curve. The curves were judged for consistency and any curves containing anomalies were removed before subsequent analysis. Fig. 5 (a-c) shows the raw output from the machine. The samples were tested using an Ultra Nano Hardness Tester (UNHT) from Anton-Paar using a Berkovich tip, which was calibrated on a fused silica standard. To ensure the indentation procedure was tuned properly for the particles embedded in LDPE, some reference tests were performed on sections of the plain LDPE. The results of M , displayed in Table S1, agree very well with the reference value of 300 MPa found in the literature (Carotenuto et al., 2012) after the conversion of plain stress to plain strain. The mechanical properties were then extracted from the resulting load-displacement curve (Fig. 5) by applying the continuum scale model of Oliver and Pharr (2011a) (see Eqs. (2)–(5)) to obtain the indentation modulus M , which represents the elastic response of the material, and hardness H , which is the resistance to permanent deformation. Note that in Fig. 5d, “bentonite + graphene” refers to indents that were performed on the bentonite layers of GHNs, whereas “graphene sheets in bentonite” refers to indents that were performed on the graphene-like sheets that formed on the surface of the GHNs.

$$M = \frac{\sqrt{\pi}}{2} \frac{S}{\sqrt{A_c(h_c)}} = \frac{E}{(1-\nu^2)} \quad (2)$$

$$S = \frac{dP}{dh} = \frac{2}{\sqrt{\pi}} E_r \sqrt{A_c} \quad (3)$$

$$\frac{1}{E_r} = \frac{(1-\nu^2)}{E} + \frac{(1-\nu_i^2)}{E_i} \quad (4)$$

$$H = \frac{P_{\max}}{A_c(h_c)} \quad (5)$$

Here, A_c is the projected contact area, which is $24.5 (h_c^2)$ for the geometry of a reference Berkovich tip (between the indenter tip and the sample surface while the load is applied). h_c is the maximum penetration contact depth, E and ν are the Young's Modulus and Poisson's Ratio of the material, respectively. S is the slope of the initial descending branch of the load-displacement curve and is given by Eq. (3), where E_r is the reduced modulus, given by Eq. (4), and E_i and ν_i are the Young's modulus and Poisson's ratio of the indenter, respectively. The indentation hardness represents a strength quantity of the material and is given by Eq. (5).

The phases found in all samples are displayed in Table S1 presented in the supporting information and shown graphically in Fig. 5 d. Samples (b-d) contained multiple phases, and in each phase, we obtained M and H . The results revealed the phases in the bentonite and GHN. Bentonite has two phases: a softer phase and a stiffer phase. GHN also has two levels of stiffness. The softer phase of GHN is composed of pyrolyzed sugar, but it is still stiffer than LDPE. The majority of the phases have a standard deviation in the modulus of less than 15%, which is typical for indentation on clay minerals (Berthonneau et al., 2017). The standard deviation of hardness is higher because the calibration of the area function is calibrated on the modulus and not the hardness. This is an encouraging result because it demonstrates that

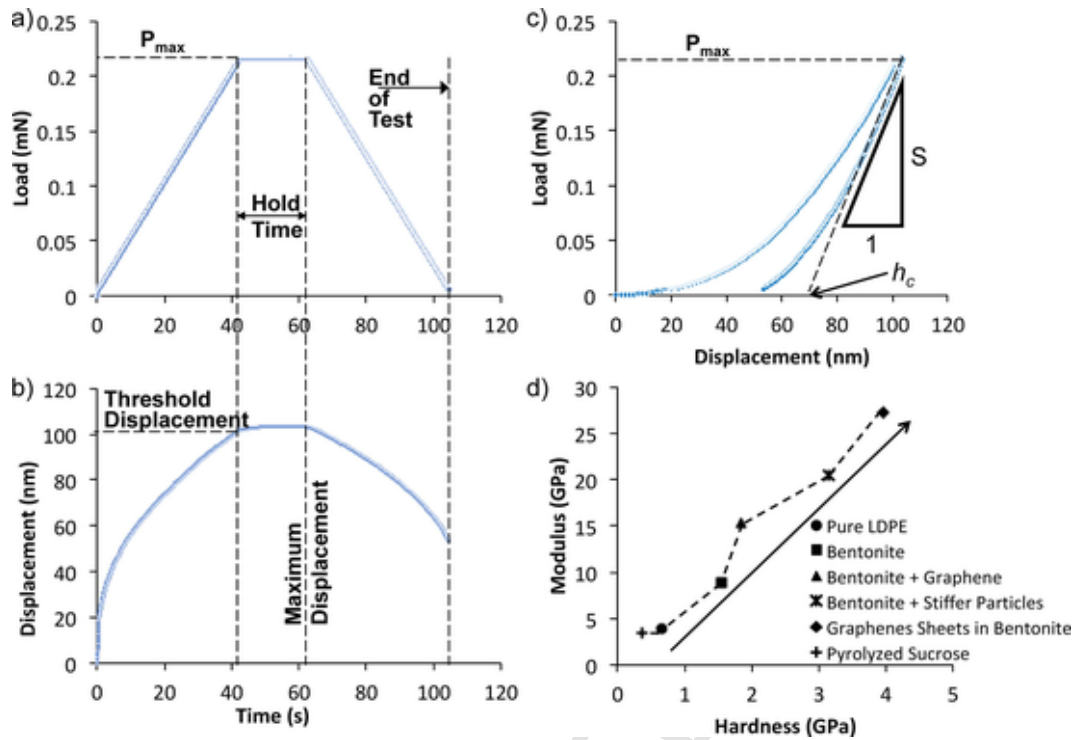


Fig. 5. Typical mechanical response to indentation; (a–c) an indent in the bentonite phase of GHN; (a) force and (b) displacement versus time curves; (c) force versus penetration depth curve (indentation modulus (M) and hardness (H) are calculated from this raw data using equations from the well-known Oliver and Pharr Model (Miller et al., 2008; Oliver and Pharr, 2011a); d) M vs H plot showing that an increase in M is accompanied by an increase in H (the dashed lines are only to guide the eyes).

the M and H values of each phase are different enough that they can be uniquely mechanically identified. The elastic modulus measured for bentonite is slightly higher than that of pure montmorillonite (Carrier et al., 2016) because bentonite is a rock that contains other minerals. The results revealed various phases. First, particles that appear to be bentonite could be identified in all samples. Sample (b) contained a bentonite-like phase that was very stiff, which is attributed to the inclusion of particles (likely SiO_2 according to mineralogy; see Table S1). Sample GHN contained enough production of graphene-like sheets both within and independent of the bentonite. In the sample, we found some graphene sheets sitting on top of the bentonite, which produced a composite response homogenized between the stiffness of the bentonite and the carbon sheets independently. One additional phase was discovered in a sample GHN, which had a modulus of approximately 3.4 GPa. This phase was attributed to pyrolyzed sucrose, as it was dark in color and there was likely a surplus of sucrose that did not contribute to the formation of graphene-like layers within the bentonite. However, this carbon contributed to the increased electrical conductivity (Boussaboun et al., 2017). The stiffness of many sugars with zero porosity has been found to be in the range from 11 to 18 GPa (Bassam et al., 1990). Since this sugar was pyrolyzed, it is reasonable for it to have a lower stiffness. While the graphene-like layers present within the bentonite are too small to be locally identified by indentation, the tests demonstrate that once GHN has formed in the bentonite, the overall stiffness increases, indicating a homogenized response of the reference bentonite and the independent graphene-like sheets.

3.3. Organic dye adsorption tests

3.3.1. Adsorption capacity comparison between GHN and BT

The efficiency of the novel synthesized graphene-like hybrid nano-materials was evaluated for removal of harmful cationic (methylene blue, MB and rhodamine B, Rh B) and anionic (methyl orange, MO), from aqueous solutions and compared to that of the template, bentonite

(BT). As can be seen in Fig. 6, the presence of graphene layers in the bentonite network provides higher adsorption capacity and faster rate than the pure bentonite clay for the three organic dyes. This enhancement in the adsorption efficiency of dyes can be explained by the increase of both number of active sites and specific surface area. XPS results have shown that GHN surface exhibits abundant hydrophilic functional groups such as the hydroxyl, carboxyl, and epoxy groups as well as sp^2 hybridized carbon atoms which could generate electrostatic interactions, hydrogen bonds, and π - π binding (Xiao et al., 2016). In addition, BET specific surface area of GHN ($267 \text{ m}^2/\text{g}$) is about three times higher than that of BT ($87 \text{ m}^2/\text{g}$). This is due to the nano-sandwich structure of GHN formed from graphene and bentonite layers.

3.3.2. Parametric effects on adsorption

In order to determine the influence of pH on adsorption, its effect on the zeta potential of both BT and GHN was investigated over the range of pH 2–10 (Fig. 7). Contrary to that of BT, the zeta potential of the GHN is remarkably influenced by the change of pH solution since it

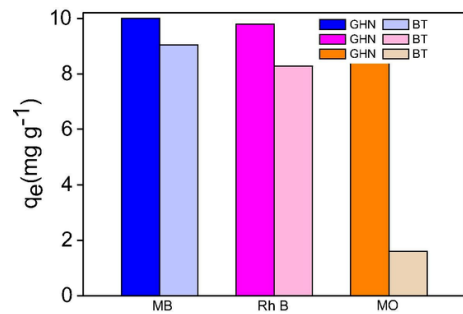


Fig. 6. Comparison between the removal capacities of BT and GHNs for cationic (MB & RhB) and anionic dye (MO) according to the adsorption time with weight of both BT and GHN are of 25 mg, initial concentration for MB, RhB, and MO is of 25 mg L^{-1} and pH of dye solutions is of 5.

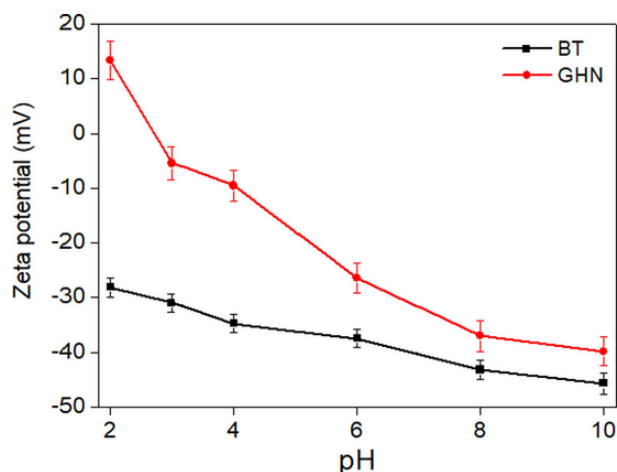


Fig. 7. Zeta potential versus pH of BT and synthesized GHN. The error bars were calculated at least five measurements for each pH.

decreased significantly at elevated pH, and the isoelectric point (IEP) was found to occur at around 2.7 (Fig. 7). This indicates that below pH 2.7, GHN surface has a positive charge in solution and a negative charge above this pH, which is explained primarily by the presence of acidic groups, i.e. carboxylic acid and hydroxyl, on the surface of the graphene particles which are protonated at highly acidic media and deprotonated at basic solutions (Perreault et al., 2015).

To determine the optimal conditions for dye removal efficiency, the effects of pH and temperature were examined (Fig. S1 shown in the supporting information). The GHN adsorption capacity for removal of cationic and anionic dyes as a function of the initial pH is shown in Fig. S1a. The results suggest that the adsorption of MB and RhB is insignificantly affected by pH indicating no noticeable charge interaction between MB, RhB and GHN. Thus, one can predict that the adsorption of MB and RhB cationic dyes on GHN is mainly dominated by π - π interaction. In contrast, the adsorption of MO, as an example of anionic dye, decreased continuously as the maximum adsorbed amount was obtained at pH 2 (9.65 mg g^{-1}) and the minimum at pH 10 (1.48 mg g^{-1}). This is due to electrostatic attraction between the anionic dye and the positively charged GHN for pH value below 2.7 and electrostatic repulsion at pH higher than this IEP value. Moreover, at alkaline pH, adsorption of OH^- ions could compete effectively with the dye anion adsorption resulting in a decrease in removal of the MO.

To investigate thermodynamics of the dyes adsorption, 25 mg GHN were dispersed in 10 mL of each dye solution separately at 25 mg L^{-1} concentration for 1 h at four temperatures ranging from 25 to 50 °C, and the obtained adsorption results are shown in Fig. S1b. As we can observe, MB was fully adsorbed on GHN (10 mg g^{-1}) at all studied temperatures, indicating strong MB-GHN affinity. While RhB and MO adsorption increased gradually with increasing temperature, revealing an endothermic nature of the adsorption process and showing that high temperature was favorable for adsorption of these dyes. The thermodynamic parameters dealing with enthalpy change (ΔH°), entropy change (ΔS°), and Gibbs's free energy change (ΔG°) are calculated based on van't-Hoff Eq. (6). ΔH° and ΔS° were evaluated respectively from the slope and intercept of the linear van't-Hoff plot of $\ln K$ versus $1/T$ (Eq. (2)). Whereas ΔG° was calculated using equation (Eq. (7)), and K was determined using Eq. (8).

$$\ln K = \frac{\Delta S^\circ}{R} - \frac{\Delta H^\circ}{RT} \quad (6)$$

$$\Delta G^\circ = -RT \ln K \quad (7)$$

$$K = \frac{q_e}{C_e} \quad (8)$$

where K (L g^{-1}) is the thermodynamic equilibrium constant calculated with Eq. (7), R ($8.314 \text{ J mol}^{-1} \text{ K}^{-1}$) is the universal gas constant, T (K) is the temperature, C_o (mg L^{-1}) is the initial concentration of dyes, C_e (mg L^{-1}) is the concentration of dyes at equilibrium, V (L) is the volume of the solution, m (g) is the used mass of adsorbent.

From the calculated thermodynamic parameters recapitulated in Table S2 shown in the supporting information, one can note that the values of ΔG° are negative which predict a spontaneous transfer process of the three dye molecules from the solution to GHN adsorbent surface, and that absolute values of ΔG° of cationic dye are much higher than those of the anionic one revealing higher adsorption capacities should be expected for cationic dyes. The positive value of ΔH° suggests that the process of adsorption of the studied dyes under the operation conditions was of endothermic nature and the positive value of ΔS° indicates an increase in disorder at the interface adsorbent solution referring to the randomness of the adsorption reaction (Wang et al., 2017).

3.3.3. Adsorption isotherms and kinetics

The adsorption of both cationic and anionic dyes fitted best Langmuir models (Table 1). The Langmuir isotherm describes a monolayer dye adsorption on the outer surface of the adsorbent, and the Freundlich model describes a multilayer adsorption on heterogeneous surface. The K , K_F , and $1/n$ parameters characterize the adsorbent – adsorbate interactions and are dependent on the surface chemical composition. In the Freundlich model, a $1/n$ value below one indicates a monolayer chemisorption mode, as is observed for RhB and MB. In contrast a value above one, as observed in the case of MO, indicates a cooperative adsorption and deviation from the Langmuir model (Foo and Hameed, 2010). In comparison with other graphene-based materials, the prepared GHN composite exhibits excellent adsorption abilities for different organic dyes. The detailed comparison is summarized in Table 2. The maximum adsorption capacity obtained from the Langmuir model for MB, RhB and MO are 455 mg g^{-1} , 53 mg g^{-1} and 69 mg g^{-1} respectively, indicating that GHN could be used efficiently in water treatment. Electrostatic forces have a strong influence on the adsorption and, in agreement with the conclusions of the zeta potential results discussed earlier, as well as the pi-pi stacking interactions, which are stronger for the two cationic dyes. The adsorption kinetics of the three dyes fitted well the pseudo-second-order model that the adsorption is mainly controlled by a chemical process. The sorption of RhB can be accordingly described by *pseudo-first* and *pseudo-second-order* kinetics, represented by high values of linear coefficients (>0.9) while the pseudo-second order kinetic was suitable for describing the sorption of MB.

3.3.4. Adsorbent recyclability

To demonstrate the practical application of this new adsorbent for dye removal from water, the regeneration and the reusability of the GHN adsorbent were tested. Water contaminated with MB as an example of model dyes was used for five repeated experiments of adsorp-

Table 1
Isotherms parameters for the adsorption of MB, Rh B, and MO dyes on GHN adsorbent.

Dye	Experimental q_e (mg g^{-1})	Langmuir		Freundlich			
		R^2	$K \cdot 10^3$ (L mg^{-1})	q_m (mg g^{-1})	R^2	K_F (mg g^{-1})	$1/n$
MB	10.00	1.000	01.00	455	0.999	1.482	0.99
RhB	9.97	0.998	0.300	53	0.991	2.600	0.16
MO	9.56	0.915	0.285	69	0.818	0.260	1.85

Table 2
Dye adsorption capacity of some graphene-based composites.

Adsorbent	Dye	Adsorption capacity (mg.g ⁻¹)	Reference
GHN	MB	455	This work
Exfoliated graphene		500	(Xue et al., 2016)
Carbon nanotube-Graphene aerogel		191	(Sui et al., 2012)
Magnetic chitosan- Graphene Oxide		181	(Fan et al., 2012)
Reduced Graphene oxide sponge		184	(Zhao et al., 2012)
PVA/CMC hydrogels-Graphene Oxide/Bentonite		172	(Dai et al., 2018)
GHM	RhB	53	This work
Reduced Graphene oxide/Fe ₃ O ₄		37–41	(Geng et al., 2012)
Reduced Graphene oxide sponge		73	(Zhao et al., 2012)
Carbon nanotube-Graphene aerogel		150	(Sui et al., 2012)
GHN	MO	69	This work
Reduced Graphene oxide sponge		12	(Zhao et al., 2012)

tion/desorption cycles. For desorption of MB dye and regeneration of the adsorbent, filtration was first used in order to separate GHN adsorbent powder from the aqueous dye solution, followed by an abundant washing using 1 M HCl solution and then by a drying at 80 °C under vacuum. As can be observed in Fig. 8, GHN adsorbent did not show loss of adsorption capacity for the three first adsorption cycles, and a very slight loss was observed up to five cycles. This proved its high stability and facile regeneration of the developed hybrid sorbent.

4. Conclusions

Graphene-like hybrid nanomaterials have been successfully prepared from renewable sucrose and bentonite clay using an eco-friendly, solvent-free approach. The synergy between the hybrid clay-graphene surface chemistry and the high specific surface area of the composites make these materials well suited for surface dependent applications, such as the removal of pollutants from aqueous media. The characterization methods showed the presence of the graphene in the clay. The presence of the graphene was shown to drastically improve the mechanical properties of the bentonite particles. The prepared GHN exhibits adsorption ability toward model pollutants methylene blue, rhodamine B, and methyl orange. The removal of the positively charged dyes by the negatively charged adsorbent occurs via ion exchange mechanism through electrostatic interactions. This work demonstrates

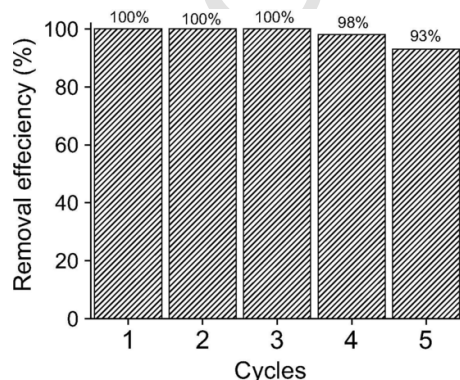


Fig. 8. Reusability test of GHN adsorbent for MB removal from water up to five cycles.

a simple and cost-effective method to prepare graphene-like hybrid nanomaterials. The stiffer and more adsorbent particles are well suited for water treatment, especially for applications in high flow filters where the forces on the particles will undoubtedly be high.

Funding

The Natural Sciences and Engineering Council of Canada and Quebec Centre for Advanced Materials (QCAM/CQMF) from Fonds de recherche du Québec – Nature et technologies partly funded this study.

Declaration of Competing Interest

The authors declare that they have no known competing financial interests or personal relationships that could have appeared to influence the work reported in this paper.

Appendix A. Supplementary data

Supplementary data to this article can be found online at <https://doi.org/10.1016/j.ces.2021.116482>.

References

- Al-Hamadani, Y.A.J., Jung, C., Im, J.-K., Boateng, L.K., Flora, J.R.V., Jang, M., Heo, J., Park, C.M., Yoon, Y., 2017. Sonocatalytic degradation coupled with single-walled carbon nanotubes for removal of ibuprofen and sulfamethoxazole. *Chem. Eng. Sci.* 162, 300–308.
- An, Y.-X., Qu, W.-J., Yu, P.-Z., Lü, J.-G., 2018. The assembly of a composite based on nano-sheet graphene oxide and montmorillonite. *Pet. Sci.* 15 (2), 366–374.
- Azizi, S., C. Ouellet-Plamondon, E. David and M. F. Fréchet, 2017. Electrical and thermal properties of low-density polyethylene/graphene-like composite. 2017 IEEE Conference on Electrical Insulation and Dielectric Phenomenon (CEIDP) 517–520. doi:10.1109/CEIDP.2017.8257637. <https://ieeexplore.ieee.org/abstract/document/8257637>.
- Azizi, Sohrab, C. Ouellet-Plamondon, P. Nguyen-Tri, M. Fréchet and E. David, 2019. Electrical, thermal and rheological properties of low-density polyethylene/ethylene vinyl acetate/graphene-like composite. *Composites Part B: Engineering* 107288, 107288. doi:<https://doi.org/10.1016/j.compositesb.2019.107288>.
- Bassam, F., York, P., Rowe, R.C., Roberts, R.J., 1990. Young's modulus of powders used as pharmaceutical excipients. *Int. J. Pharm.* 64 (1), 55–60.
- Berthonneau, J., Hoover, C.G., Grauby, O., Baronnet, A., Pellenq, R.J.M., Ulm, F.-J., 2017. Crystal-chemistry control of the mechanical properties of 2:1 clay minerals. *Appl. Clay Sci.* 143, 387–398.
- Bi, H., Wan, S., Cao, X., Wu, X., Zhou, Y., Yin, K., Su, S., Ma, Q., Sindoro, M., Zhu, J., Zhang, Z., Zhang, H., Sun, L., 2019. A general and facile method for preparation of large-scale reduced graphene oxide films with controlled structures. *Carbon* 143, 162–171.
- Bouakaz, B.S., Pillin, I., Habi, A., Grohens, Y., 2015. Synergy between fillers in organomontmorillonite/graphene-PLA nanocomposites. *Appl. Clay Sci.* 116–117, 69–77.
- Bouakaz, B.S., Habi, A., Grohens, Y., Pillin, I., 2017. Organomontmorillonite/graphene-PLA/PCL nanofilled blends: new strategy to enhance the functional properties of PLA/PCL blend. *Appl. Clay Sci.* 139, 81–91.
- Boussaboun, Z., Azizi, S., Ouellet-Plamondon, C.M., 2017. In: *Conductive clay containing graphene layers*, 2017 IEEE 17th International Conference on Nanotechnology (IEEE-NANO), 25–28 July 2017, pp. 1065–1069.
- Carotenuto, G., Nicola, S.D., Palomba, M., Pullini, D., Horswell, A., Hansen, T.W., Nicolais, L., 2012. Mechanical properties of low-density polyethylene filled by graphite nanoplatelets. *Nanotechnology* 23 (48), 485705.
- Carrier, B., Vandamme, M., Pellenq, R.J.M., Bomert, M., Ferrage, E., Hubert, F., Van Damme, H., 2016. Effect of water on elastic and creep properties of self-standing clay films. *Langmuir*.
- Chen, X., Lai, D., Yuan, B., Fu, M.-L., 2019. Tuning oxygen clusters on graphene oxide to synthesize graphene aerogels with crumpled nanosheets for effective removal of organic pollutants. *Carbon* 143, 897–907.
- Cheng, W., Ding, C., Nie, X., Duan, T., Ding, R., 2017. Fabrication of 3D macroscopic graphene oxide composites supported by montmorillonite for efficient U(VI) wastewater purification. *ACS Sustainable Chem. Eng.* 5 (6), 5503–5511.
- Chyan, Y., Ye, R., Li, Y., Singh, S.P., Arnusch, C.J., Tour, J.M., 2018. Laser-induced graphene by multiple lasing: toward electronics on cloth, paper, and food. *ACS Nano* 12 (3), 2176–2183.
- Dai, H., Huang, Y., Huang, H., 2018. Eco-friendly polyvinyl alcohol/carboxymethyl cellulose hydrogels reinforced with graphene oxide and bentonite for enhanced adsorption of methylene blue. *Carbohydr. Polym.* 185, 1–11.
- Eckmann, A., Felten, A., Mishchenko, A., Britnell, L., Krupke, R., Novoselov, K.S., Casiraghi, C., 2012. Probing the nature of defects in graphene by Raman spectroscopy. *Nano Lett.* 12 (8), 3925–3930.
- Fan, L., Luo, C., Sun, M., Li, X., Lu, F., Qiu, H., 2012. Preparation of novel magnetic chitosan/graphene oxide composite as effective adsorbents toward methylene blue. *Bioresour. Technol.* 114, 703–706.
- Foo, K.Y., Hameed, B.H., 2010. Insights into the modeling of adsorption isotherm systems. *Chem. Eng. J.* 156 (1), 2–10.

- Geng, Z., Lin, Y., Yu, X., Shen, Q., Ma, L., Li, Z., Pan, N., Wang, X., 2012. Highly efficient dye adsorption and removal: a functional hybrid of reduced graphene oxide-Fe₃O₄ nanoparticles as an easily regenerative adsorbent. *J. Mater. Chem.* 22 (8), 3527–3535.
- Jastuja, K., Linn, J., Melton, S., Berry, V., 2010. Microwave-reduced uncapped metal nanoparticles on graphene: tuning catalytic, electrical, and Raman properties. *J. Phys. Chem. Lett.* 1 (12), 1853–1860.
- Krstić, V., Urošević, T., Pešovski, B., 2018. A review on adsorbents for treatment of water and wastewaters containing copper ions. *Chem. Eng. Sci.* 192, 273–287.
- Li, G., Quan, K., Liang, Y., Li, T., Yuan, Q., Tao, L., Xie, Q., Wang, X., 2016. Graphene-montmorillonite composite sponge for safe and effective hemostasis. *ACS Appl. Mater. Interfaces* 8 (51), 35071–35080.
- Miller, M., Bobko, C., Vandamme, M., Ulm, F.-J., 2008. Surface roughness criteria for cement paste nanoindentation. *Cem. Concr. Res.* 38 (4), 467–476.
- Oliveira, A.E.F., Braga, G.B., Tarley, C.R.T., Pereira, A.C., 2018. Thermally reduced graphene oxide: synthesis, studies and characterization. *J. Mater. Sci.* 53 (17), 12005–12015.
- Oliver, W.C., Pharr, G.M., 2011a. Measurement of hardness and elastic modulus by instrumented indentation: advances in understanding and refinements to methodology. *J. Mater. Res.* 19 (1), 3–20.
- Oliver, W.C., Pharr, G.M., 2011b. An improved technique for determining hardness and elastic modulus using load and displacement sensing indentation experiments. *J. Mater. Res.* 7 (6), 1564–1583.
- Perreault, F., Fonseca de Faria, A., Elimelech, M., 2015. Environmental applications of graphene-based nanomaterials. *Chem. Soc. Rev.* 44 (16), 5861–5896.
- Rahmani, F., Nouranian, S., 2018. Thermal analysis of montmorillonite/graphene double-layer coating as a potential lightning strike protective layer for cross-linked epoxy by molecular dynamics simulation. *ACS Appl. Nano Mater.*
- Ruan, G., Sun, Z., Peng, Z., Tour, J.M., 2011. Growth of graphene from food, insects, and waste. *ACS Nano* 5 (9), 7601–7607.
- Ruiz-Garcia, C., Perez-Carvajal, J., Berenguer-Murcia, A., Darder, M., Aranda, P., Cazorla-Amoros, D., Ruiz-Hitzky, E., 2013. Clay-supported graphene materials: application to hydrogen storage. *PCCP* 15 (42), 18635–18641.
- Ruiz-Garcia, C., Darder, M., Aranda, P., Ruiz-Hitzky, E., 2014. Toward a green way for the chemical production of supported graphenes using porous solids. *J. Mater. Chem. A* 2 (7), 2009–2017.
- Ruiz-Hitzky, E., Sobral, M.M.C., Gómez-Avilés, A., Nunes, C., Ruiz-García, C., Ferreira, P., Aranda, P., 2016. Clay-graphene nanoplatelets functional conducting composites. *Adv. Funct. Mater.* 26 (41), 7394–7405.
- Segad, M., Jonsson, B., Akesson, T., Cabane, B., 2010. Ca/Na montmorillonite: structure, forces and swelling properties. *Langmuir* 26 (8), 5782–5790.
- Shahzad, A., Jawad, A., Iftikhar, J., Chen, Z., Chen, Z., 2019. The hetero-assembly of reduced graphene oxide and hydroxide nanosheets as superlattice materials in PMS activation. *Carbon*.
- Sui, Z., Meng, Q., Zhang, X., Ma, R., Cao, B., 2012. Green synthesis of carbon nanotube-graphene hybrid aerogels and their use as versatile agents for water purification. *J. Mater. Chem.* 22 (18), 8767–8771.
- Unuabonah, E.I., Günter, C., Weber, J., Lubahn, S., Taubert, A., 2013. Hybrid clay: a new highly efficient adsorbent for water treatment. *ACS Sustainable Chem. Eng.* 1 (8), 966–973.
- Wang, J., Shen, B., Kang, D., Yuan, P., Wu, C., 2019. Investigate the interactions between biomass components during pyrolysis using in-situ DRIFTS and TGA. *Chem. Eng. Sci.* 195, 767–776.
- Wang, J., Duan, X., Dong, Q., Meng, F., Tan, X., Liu, S., Wang, S., 2019. Facile synthesis of N-doped 3D graphene aerogel and its excellent performance in catalytic degradation of antibiotic contaminants in water. *Carbon* 144, 781–790.
- Wang, L.K., Wang, M.-H.-S., Hung, Y.-T., Shammass, N.K., Chen, J.P., 2017. Handbook of advanced industrial and hazardous wastes management. CRC Press.
- Xiao, J., Lv, W., Xie, Z., Tan, Y., Song, Y., Zheng, Q., 2016. Environmentally friendly reduced graphene oxide as a broad-spectrum adsorbent for anionic and cationic dyes via π - π interactions. *J. Mater. Chem. A* 4 (31), 12126–12135.
- Xue, Z., Zhao, S., Zhao, Z., Li, P., Gao, J., 2016. Thermodynamics of dye adsorption on electrochemically exfoliated graphene. *J. Mater. Sci.* 51 (10), 4928–4941.
- Zhao, J., Ren, W., Cheng, H.-M., 2012. Graphene sponge for efficient and repeatable adsorption and desorption of water contaminations. *J. Mater. Chem.*
- Zhu, C., Guo, S., Fang, Y., Dong, S., 2010. Reducing sugar: new functional molecules for the green synthesis of graphene nanosheets. *ACS Nano* 4 (4), 2429–2437.